

© Copyright 2005 American Meteorological Society (AMS). Permission to use figures, tables, and brief excerpts from this work in scientific and educational works is hereby granted provided that the source is acknowledged. Any use of material in this work that is determined to be “fair use” under Section 107 of the U.S. Copyright Act or that satisfies the conditions specified in Section 108 of the U.S. Copyright Act (17 USC §108, as revised by P.L. 94-553) does not require the AMS’s permission. Republication, systematic reproduction, posting in electronic form on servers, or other uses of this material, except as exempted by the above statement, requires written permission or a license from the AMS. Additional details are provided in the AMS CopyrightPolicy, available on the AMS Web site located at (<http://www.ametsoc.org/AMS>) or from the AMS at 617-227-2425 or [copyright@ametsoc.org](mailto:copyright@ametsoc.org).

Permission to place a copy of this work on this server has been provided by the AMS. The AMS does not guarantee that the copy provided here is an accurate copy of the published work.

## **P4R.5 ON THE DEVELOPMENT OF A MULTI-ALGORITHM RADAR DATA QUALITY CONTROL SYSTEM AT THE NAVAL RESEARCH LABORATORY**

Paul R. Harasti\*

University Corporation for Atmospheric Research, Boulder, CO

David J. Smalley and Mark Weber

Lincoln Laboratory, Massachusetts Institute of Technology, Lexington, MA

Cathy J. Kessinger

National Center for Atmospheric Research, Boulder, CO

Qin Xu, Pengfei Zhang and Shun Liu

National Severe Storms Laboratory, Norman, OK

Ted L. Tsui, John Cook and Qingyun Zhao

Naval Research Laboratory, Monterey, CA

### **1. INTRODUCTION**

A radar data quality control (QC) system is being developed for the real-time, continuously updateable NOWCAST system at the Naval Research Laboratory (NRL-NOWCAST) in Monterey, California. NRL has developed its own new radar QC algorithms, and is also working with the MIT Lincoln Laboratory (MIT LL), the National Center for Atmospheric Research (NCAR) and the National Severe Storms Laboratory (NSSL) to obtain, adapt, integrate, test and install various types of recently-developed radar QC algorithms for use with NRL-NOWCAST. These algorithms work with volume scans of full-resolution Doppler radar data, and have recently demonstrated success at separating the radar echoes of precipitation from other echo types and artifacts, such as noise, normal and anomalous propagation (AP) ground clutter, sea clutter, insects/clear-air, birds, and constant power function (CPF) artifacts. A separate QC issue is aliased radial velocity data from precipitation and insect/clear-air returns, which if correctly de-aliased, afford the opportunity to estimate winds. NRL is also utilizing various radial velocity de-aliasing algorithms published in the literature. The goal is to test the performance of the selected echo classifying and de-aliasing algorithms on a series of archived data sets simultaneously in order to determine the optimal combination for future use with NRL-NOWCAST.

NRL-NOWCAST ingests full-resolution Doppler radar data from both the Weather Surveillance Radar-1988 Doppler (WSR-88D) network and US Department of Defense (DoD) radars, such as the Supplemental Weather Radar (SWR) at Navy shore sites, and creates various products from these data for its real-time display. The radar data is also ingested into the COAMPS-OS<sup>®\*\*</sup> (Geiszler et al. 2004) data assimilation

system at NRL. Figure 1 shows a flow chart that summarizes the processing stages and uses of radar data at NRL. Figure 2 shows an example of the NRL-NOWCAST, Fallon, NV, demonstration site, where the specific products displayed are only a few from a large list that may be chosen by the forecasters at the Naval Air Station at Fallon.

This paper presents a brief overview of the concepts behind the various echo classifying and de-aliasing algorithms under consideration. Test results from an NRL algorithm testing platform will also be presented along with some previously published test results from the authors. Additional test results from the platform will be presented at the conference.

### **2. MIT LL Data Quality Assurance (DQA) Algorithm**

DQA was originally developed for the Federal Aviation Administration to QC NEXRAD reflectivity data only, but it is currently being adapted for use with DoD radar data at NRL, and the QC is being extended to radial velocity, and spectral width data as well. These three primary radar data moments are used to identify and remove CPF artifacts and AP clutter in two sequential stages (Smalley and Bennett 2001; 2002, Smalley et al. 2003).

The CPF Detector removes calibration patterns and hardware malfunctions, such as bull's eyes and starbursts, as well as sun strobes. The detector works by searching the radar radials for a constant power signal, which has a corresponding reflectivity proportional to the square of the distance from the radar. The signal must be sufficiently continuous over a portion of the radial. Radials that have a mix of CPF artifacts and other echo types, or whose signal is not sufficiently dense, cannot have their CPF portions removed.

If minimal CPF artifacts are detected then the AP detector is applied next in a three-tiered fashion. First, range gates with high reflectivity coincident with very small radial velocity and spectrum width are identified within each single radial. Second, the detected AP gate is allowed to bloom radially to adjacent gates if those gates are sufficiently close to but not quite within the bounds of the basic test. Third, a scatter filter is applied

---

\*Corresponding author address: Dr. Paul R. Harasti, UCAR Visiting Scientist, Naval Research Laboratory, Marine Meteorology Division, On-Scene Systems Section, 7 Grace Hopper Avenue, MS-2, Monterey, CA 93943-5502.

E-mail: harasti@nrlmry.navy.mil.

\*\* COAMPS<sup>®</sup> and COAMPS-OS<sup>®</sup> are registered trademarks of the Naval Research Laboratory.

over the entire tilt of data; i.e., the sufficiency of AP neighbors from first and second steps is assessed and like-status assigned to the target central gate within the filter.

Figure 3 shows some of the results of applying the DQA CPF detector installed on the NRL development platform to two archive level II WSR-88D data sets from San Francisco, CA (KMUX) and Reno, NV (KRGX) on 28 July 2005. DQA successfully removed the bull's eye patterns within all eleven surveillance scans that comprise the volume scan of this case (only two scans shown) except for the 8 radials shown in the top right panel. Apparently, the density of the CPF signal was not sufficient to identify those radials, although radials of comparable density in the west-south-west direction were removed. MIT LL is currently working on an improved version of its artifact detector that will remove CPF signals of low density more consistently.

The bottom panels of Fig. 3 show the successful identification and removal of a sun strobe during sunrise at KRGX. The CPF detector also successfully identified and removed a similar sun strobe in the reflectivity data in the next two scans within this KRGX volume scan (not shown). Figure 4 shows an MIT LL application of the DQA AP detector to WSR-88D data from (KAMA). It is demonstrated that a significant amount of AP ground clutter can be identified and removed by the algorithm.

### 3. NCAR Radar Echo Classifier (REC) Algorithm

The current REC algorithm is tailored for NEXRAD data, and used on the WSR-88D Open Radar Product Generator system (Saffle et al. 2001) to improve radar-derived rainfall estimates and other products used by forecasters. REC uses full-resolution reflectivity, radial velocity and spectrum width data in a fuzzy logic detection algorithms to make echo-type classifications. It was developed and "truthed" using WSR-88D and NCAR S-Pol radar data, and includes four separate algorithms to detect AP Clutter, Precipitation, Insect-Clear-Air, and Sea Clutter (Kessinger et al. 2003).

Figure 5 describes the REC fuzzy logic engine, from the raw data input through to the final product of the type of echo being considered. The basic tenant underlying REC is that the feature fields indicated in the figure have unique histogram curve shapes of the fraction of range gates for each different type of radar echo, thus providing a means to distinguish between them. The histograms have been established a priori using various data sets at NCAR; the actual REC algorithm utilizes normalized membership functions that were derived from each corresponding histogram – a unique function for each type of echo and feature field. Weights are applied to the output of the membership functions and summed to generate an interest field for each echo type. A threshold is then chosen to identify the particular echo types.

Figure 6 shows an NCAR application of REC to S-Pol radar data from the International H<sub>2</sub>O Project (IHOP) field experiment on 16 June 2002. The AP detection algorithm (APDA) of REC successfully identified the portion of the echo corresponding to AP ground clutter.

The precipitation detection algorithm (PDA) also performed well by identifying the majority of the echo corresponding to precipitation, however, a small region of clear air return was incorrectly classified as precipitation. This would have no consequence to radar wind products derived from the radial velocity, however, products related to precipitation that are generated from the reflectivity would not be valid in this region of clear air return.

### 4. NSSL Radar Data QC Algorithms

NSSL has delivered a two-part QC package to NRL specifically designed for full-resolution WSR-88D data; one part deals with radial velocity de-aliasing and the other deals with unwanted echo classification and removal. NRL is currently working with NSSL to adapt their package for use with DoD radar data as well.

The de-aliasing algorithm uses the three-step algorithm of Gong et al. (2003). Step one employs modified VAD winds as reference for the first de-aliasing pass; modified VAD winds are not susceptible to aliased data but are somewhat noisier than traditional VAD winds. Traditional VAD winds are then calculated in step two for both a horizontal averaging and variance check, and a vertical shear check, leading to a refined radial velocity reference field and another de-aliasing attempt. The boundaries of the residual aliased data are also located and flagged by the large differences between their values and the adjacent de-aliased data. In step three, the areas of de-aliased data outside the bounds of the residual regions of aliased data are used as a continuity check from all radial and azimuthal directions around the residual regions to de-alias them. Figure 7 shows an example of this algorithm applied to the aliased radial velocity data of a mesocyclone observed by the Norman, OK (KTLX) WSR-88D on 1999 May 4.

The NSSL echo classifier and removal algorithm uses QC parameters (feature fields) derived from reflectivity and radial velocity, similar to the NCAR REC algorithm. Some of the QC parameters calculated are: the percentage of along-beam sign changes of radial velocities (SN), the along-beam standard deviation of radial velocities (STD), the percentage of along-beam perturbation radial-velocity sign changes (VSC), valid radial-velocity data coverage (VDC), and mean reflectivity (MRF). Thresholds for these parameters are determined based on accumulated statistics (probability distribution functions) and classified for the different WSR-88D Volume Coverage Patterns (scan types). Large SN (> 15%) and/or STD (> 3 m s<sup>-1</sup>) identify regions of noisy data fields (Liu et al. 2003). Fuzzy logic of these QC parameters is also used to detect AP clutter from both stationary clutter and moving vehicles.

Large circular regions of migrating birds can often be seen in radar images during the evening in the spring and autumn. As figure 8 shows, this can be a near-simultaneous and very widespread problem across the United States. Regions of large SN, MRF and VDC indicate a high probability of contamination by migration birds (Zhang et al. 2005). The NSSL bird echo removal

algorithm utilizes probability distribution functions (PDF) of the QC parameters derived from accumulated statistics of situations where the radar data either is, or is not, contaminated by birds. Bayes conditional probability theorem is then used to determine the two probabilities of these situations. Figure 9 shows an example of the PDF for the QC parameter MRF along with verification statistics, which show that migrating birds are most accurately located in the radar scan when the statistics are derived from the multi-parameters MRF, VDC and VSC.

## 5. Principal Component Analysis (PCA) QC

Harasti (2000) and Harasti and List (2005) show the first application of PCA to Doppler weather radar data. Although these studies focused on the so-called *PCA analysis* approach of seeking physical interpretations of the eigen analysis results involved in PCA, the potential of the reverse approach – *PCA synthesis* – was also discussed. In brief, PCA synthesis involves the following equation:

$$\mathbf{D} \approx \mathbf{PE}^T + \mathbf{Id}. \quad (1)$$

For the case of Doppler radar data,  $\mathbf{D}$  is the  $N \times M$  matrix of radial velocity data (or any other radar data type), where  $N$  is the number of range gates and  $M$  is the number of azimuth positions within a single surveillance scan at fixed elevation angle.  $\mathbf{P}$  and  $\mathbf{E}$  are the  $N \times K$  and  $M \times K$  matrices of principal components and eigenvectors, respectively, of the covariance matrix of  $\mathbf{D}$ , where “T” signifies the matrix transpose operation and  $K$  is number that signifies that *the first K* principal components and eigenvectors from the PCA are contained in  $\mathbf{P}$  and  $\mathbf{E}$ , respectively. The outer (vector) product of each  $N$ -element principal component stored in the columns of  $\mathbf{P}$ , and its associated  $M$ -element eigenvector in the corresponding column of  $\mathbf{E}$ , represent a particular proportion of the total variance of  $\mathbf{D}$ , and they are stored sequentially in  $\mathbf{P}$  and  $\mathbf{E}$  in descending order of their proportion of variance representation.  $\mathbf{I}$  is the  $N \times M$  identity matrix, and  $\mathbf{d}$  is an  $M$ -element vector containing the separate averages of each column of  $\mathbf{D}$ . When  $K = \min(N-1, M)$  is used in (1), the original matrix  $\mathbf{D}$  is exactly reproduced, thus the origin of the term *PCA synthesis*. However, for the current application, the idea is to choose some value of  $K \ll \min(N-1, M)$  that approximates  $\mathbf{D}$  to sufficient accuracy, preferably a value that separates the signal from the noise and clutter as closely as possible.

In effect, the approximation (1) simultaneously provides the ordinate values of  $N$  curve-fits in the radial direction, and  $M$  curve fits in the azimuthal direction at the fixed abscissa points of the range and azimuth coordinates, respectively. The curve fits in the azimuthal direction are similar to Velocity Azimuth Display (VAD) approximation of Browning and Wexler (1968); the difference is in the basis functions used. The basis functions of PCA are the eigenvectors of  $\mathbf{E}$ , also known as Empirical Orthogonal Functions; i.e., natural, data-derived basis functions. On the other hand, the basis functions of the VAD method are the harmonics within a truncated Fourier series. The main advantage of using

(1) over a fit provided by the VAD method is that the VAD method attempts to fit the weather signal, clutter and non-Gaussian noise together, whereas an appropriately chosen  $K$  value in (1) can result in a fit largely representative of the weather signal, as long as the weather signal is the dominant component.

As an example of the great potential of the technique of PCA synthesis, Fig. 10 shows images of some of the radial velocity data of Hurricane Bret (1999) used in an application of (1) by Harasti and List (2001). Hurricane Bret was a category four hurricane before it weakened to a category three hurricane a few hours before landfall along the Texas coast on 22 August 1999. Two WSR-88D coastal radars located at Corpus Christi (KCRP) and Brownsville (KBRO), Texas, made near-simultaneous observations of Bret. Figure 11 shows the individual percentages of the total variance represented by each principal component-eigenvector pair in  $\mathbf{P}$  and  $\mathbf{E}$ . Apparently, the first four eigenvectors cumulatively account for over 75% (85%) of the total variance in the KBRO (KCRP) radial velocity data found in the  $0.5^\circ$  elevation surveillance scan.

There are several ways to estimate  $K$ . The current method uses the broken stick model approach described in Jolliffe (1986). Applying this approach to all 14 (11) elevation scans from the KCRP (KBRO) volumes scans near 2343 UTC results in  $K$  values of either 3 or 4 for KCRP and  $5 \leq K \leq 9$  for KBRO. These differences are likely due to the greater amount of missing sectors of data in the scans from KBRO. With the particular value of  $K$  set in (1), one can either replace the original data matrices  $\mathbf{D}$  of each elevation scan with their approximations given by (1), or use (1) to identify clutter and noise in the original data set. The latter approach was utilized by Harasti and List (2001) since they required the original data for high-order ( $\sim 10$  wavenumber) VAD fits that provided Fourier coefficients related to the hurricane wind field. However, these VAD fits were not capable of removing a large portion of the clutter and noise outliers when using a two standard deviation (or any other multiple of the standard deviation) threshold tolerance of data deviating from the VAD curves, particularly for the poorer data coverage case of KBRO. In contrast, Harasti and List (2001) found the approximation given by (1), along with a two standard deviation threshold tolerance of data deviating from the curves provided by (1), very capable of separating most of the weather signal from the noise and clutter. Figure 12 shows examples of successful PCA QC outlier rejection in the VAD data at different ranges from KCRP and KBRO. Once identified as an outlier via the PCA QC method, the reflectivity and spectrum width data corresponding to the rejected radial velocity data may also be rejected.

## 6. The Current NRL QC Approach

As Fig. 1 summarizes, the current NRL QC approach involves a three-step process. The first step removes noise and nearby clutter by applying empirically determined thresholds on the data. The thresholds involving the spectrum width and signal to noise ratio

remove noise, whereas the threshold on the range and the requirement of mutually, non-missing reflectivity and radial velocity in co-existing scans (hereafter, NMCO requirement) deal with clutter and second trip echoes. The threshold on range can be relaxed in situations of minimal ground clutter when the radar is situated onboard a ship at sea, but is employed over land to avoid radar data of poor quality that is often found close to ground-based radars, and which the current de-aliasing algorithm (to be described below) is sensitive to.

The second step of the current NRL QC approach is a new ground clutter removal algorithm recently developed at NRL by the first author. It is a simple, yet oftentimes an effective technique. Rather than reject all radial velocity values near the value of zero in a popular broad-brush technique of removing ground clutter (e.g. Matejka and Srivastava 1991), the new method compares the amount of near-zero radial velocity data in each VAD circle of data against the amount of near-zero data theoretically expected for a given wind field. For threshold calculation purposes, the wind field is assumed to be uniform across the expanse of the VAD circles, which is oftentimes a reasonable approximation in stratiform precipitation. If  $\eta$  represents the ratio of near-zero (say,  $1.5 \text{ m s}^{-1}$  in absolute magnitude) radial velocity data to the speed of the uniform wind, then one can show that the expected fraction of near-zero radial velocities around a given VAD circle is

$$F = \frac{\left(\frac{\pi}{2} - \cos^{-1} \eta\right)}{\frac{\pi}{2}}. \quad (2)$$

$\eta$  is given a value of 0.15 in the current approach, based on an assumed average wind speed of  $10 \text{ m s}^{-1}$ , however, SkewT data from a numerical model or observations could be used to specify  $\eta$  more precisely for varying wind speed conditions at different VAD circle altitudes. Only those VAD circles that contain an actual fraction of near-zero radial velocities that exceeds the theoretical value given by (2) have their near-zero radial velocities removed, along with their corresponding reflectivity and spectrum width data. Of course, the near-zero radial velocities data points associated with the weather signal within these particular VAD circles will also be removed in this scheme for the greater good of removing the oftentimes more significant numbers of clutter data points; e.g., Fig. 12b.

The third step of the current NRL QC approach de-aliases the radial velocity data using algorithm B of the Bergen and Brown (1980) technique. This technique is applied gate-by-gate, starting with an initial radial velocity estimate at the first gate. A reference wind field calculated from the gradient VAD (GVAD) method of Gao et al. (2004) is used for the initialization. If GVAD winds are not available due to an insufficient amount of data then SkewT winds from COAMPS-OS<sup>\*\*\*\*</sup> are utilized as a reference instead. Similar to the modified

VAD method of Gong et al. (2003), GVAD winds are not affected by aliased data and may be somewhat more accurate than the modified VAD winds.

Figure 13 shows examples of the application of the current NRL QC approach to SWR data from Point Loma, CA and Fallon, NV. The results from the Point Loma example show the effectiveness of both the NMCO requirement at removing the second trip echoes in this case, and the new ground clutter removal algorithm at removing anomalous propagation sea and ground clutter. Examples of the removal of normal propagation ground clutter and correctly de-aliased radial velocities are shown in the results from Fallon.

## 7. Summary and Future Work

Table 1 summarizes the target radar echoes of each algorithm described in this paper. Future work will include 1) the preparation of all the QC algorithms for use with both WSR-88D and DoD Radar data received at NRL, 2) the testing all the QC algorithms on a series of case studies and the accumulation of performance statistics according to each algorithm's echo target type, and 3) the determination the optimal combination, in a layered sequence, of the QC algorithms (either complete, partial or no components) that optimizes the quality of the radar data for COAMPS-OS<sup>®</sup> and NRL-NOWCAST. For example, it is envisioned that the NCAR REC algorithm could potentially be used in conjunction with the PCA QC method, where the classified regions of precipitation and insects/clear-air identified by REC would be re-analyzed using the PCA QC method to remove any residual clutter left by REC. This would ensure that PCA QC is only used in situations dominated by weather signal.

## 8. ACKNOWLEDEMENTS

This research is supported by the Office of Naval Research under PE 0602435N Projects 3532, BE-35-2-56 and BE-235-00. The Natural Sciences and Engineering Research Council of Canada, the Meteorological Service of Canada, the University of Toronto Open Doctoral Fellowship program (Canada), the Ontario Graduate Scholarship program (Canada) and the National Center for Atmospheric Research sponsored the development of the PCA QC method. The National Center for Atmospheric Research is sponsored by the National Science Foundation. The first author would like to thank Professor Roland List of the Department of Physics, University of Toronto, for his continued support of the development of the PCA QC method.

## 9. REFERENCES

- Bergen D. W., and R. C. Brown, 1980: Interactive radar velocity unfolding. Preprints, *19th Conference on Radar Meteorology*, Miami Beach, FL, Amer. Meteor. Soc., 278-285.
- Browning, K. A., and R. Wexler, 1968: The determination of kinematic properties of a wind field using Doppler radar. *J. Appl. Meteor.*, **7**, 105-113.

\*\*\*\*COAMPS<sup>®</sup> and COAMPS-OS<sup>®</sup> are registered trademarks of the Naval Research Laboratory.

- Gao, J., K. K. Droegemeier, J. Gong, and Q. Xu. 2004: A method for retrieving mean horizontal wind profiles from single-Doppler radar observations contaminated by aliasing. *Mon. Wea. Rev.*, **132**, 1399–1409.
- Geiszler, D., J. Kent, J. Strahl, J. Cook, G. Love, L. Phegley, J. Schmidt, Q. Zhao, F. Franco, L. Frost, M. Frost, D. Grant, S. Lowder, D. Martinez, and L. N. McDermid, 2004: The Navy's on-scene weather prediction system, COAMPS-OS®. Preprints, *20th International Conference on Interactive Information and Processing Systems for Meteorology (IIPS), Oceanography, and Hydrology*, Seattle, WA, Amer. Meteor. Soc., P19.1.
- Gong, J., L. Wang, and Q. Xu, 2003: A three-step dealiasing method for Doppler velocity data quality control. *J. Atmos. Oceanic Tech.*, **20**, 1738-1748.
- Harasti, P. R., 2000: Hurricane properties by principal component analysis of Doppler radar data. Ph.D. dissertation, Department of Physics, University of Toronto, 162 pp.
- Harasti, P. R., and R. List, 2001: The hurricane-customized extension of the VAD (HEVAD) method: Wind field estimation in the planetary boundary layer of hurricanes. Preprints, *30th Conf. on Radar Meteorology*, Munich, Germany, Amer. Meteor. Soc., 463-465.
- Harasti, P. R., and R. List, 2005: Principal component analysis of Doppler radar data. Part I: Geometric connections between eigenvectors and the core region of atmospheric vortices. *J. Atmos. Sci.* (in press).
- Jolliffe, I. T., 1986: *Principal Component Analysis*. Springer-Verlag New York Inc., 271 pp.
- Kessinger, C., S. Ellis, and J. Van Andel, 2003: The radar echo classifier: A fuzzy logic algorithm for the WSR-88D. Preprints-CD, *3rd Conference on Artificial Applications to the Environmental Science*, Long Beach, CA, Amer. Meteor. Soc.
- Liu, S., P. Zhang, L. Wang, J. Gong, and Q. Xu, 2003: Problems and solutions in real-time Doppler wind retrievals. Preprints, *31th Conference on Radar Meteorology*, 6–12 August 2003, Seattle, Washington, Amer. Meteor. Soc., 308-309.
- Liu, S., Q. Xu, and P. Zhang, 2005: Quality control of Doppler velocities contaminated by migrating birds. Part II: Bayes identification and probability tests. Submitted to *J. Atmos. Oceanic Technol.* (in press).
- Matejka, T, and R. C. Srivastava, 1991: An improved version of the extended velocity-azimuth display analysis of single-Doppler radar data. *J. Atmos. Oceanic Tech.* **8**, 453–466.
- Saffle, R.E., M.J. Istok, and L.D. Johnson, 2001: NEXRAD open systems - progress and plans. Preprints: *30th Conf on Radar Meteorology*, Munich, Amer. Met. Soc., 690-693.
- Smalley, D.J., and B.J. Bennett, 2001: Recommended improvements to the Open RPG AP-Edit algorithm. MIT Lincoln Laboratory Wx Project Memorandum No. 43PM Wx-0081, November 2001. MIT Lincoln Laboratory, Lexington, MA. 37 pp.
- Smalley, D.J., and B.J. Bennett, 2002: Using ORPG to enhance NEXRAD products to support FAA Critical Systems. Preprints, *10th Aviation, Range, and Aerospace Meteorology Conference*, Portland, OR, Amer. Meteor. Soc., 3.6.
- Smalley, D.J., B.J. Bennett and M. L. Pawlak, 2003: New products for the NEXRAD ORPG to support FAA Critical Systems. Preprints, *19th International Interactive Processing Systems Conference*, Long Beach, CA, Amer. Meteor. Soc., 14.12.
- Zhang, P., S. Liu, and Q. Xu, 2005: Quality control of Doppler velocities contaminated by migrating birds. Part I: Feature extraction and quality control parameters. *J. Atmos. Oceanic Technol.* (in press).

### NRL Radar Data Flowchart

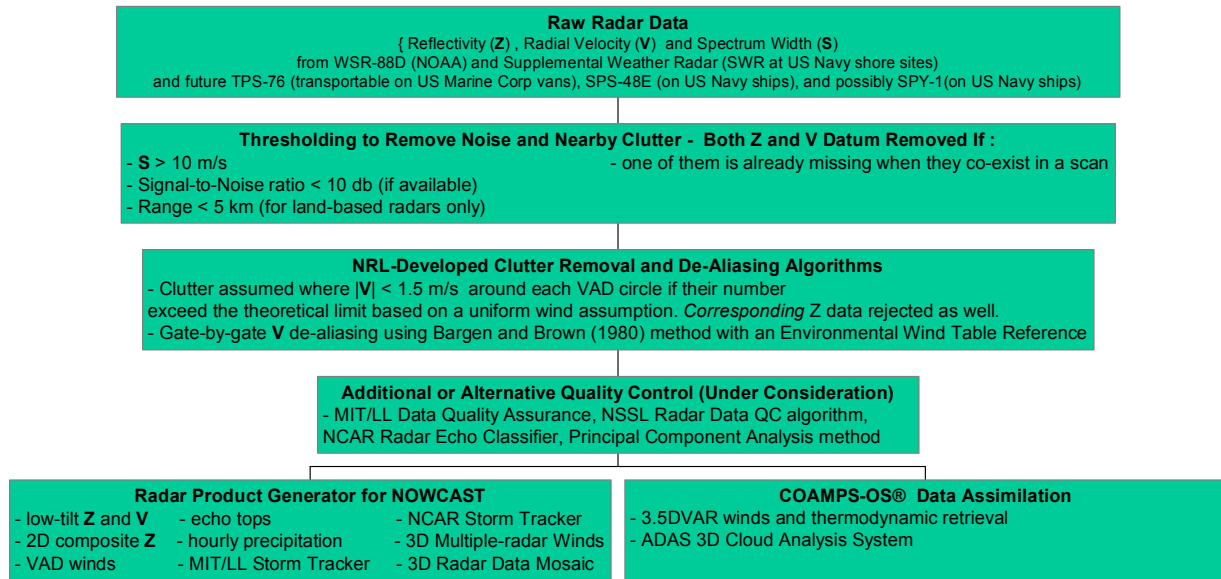


Fig. 1. Flow chart showing both the current and potential future processing stages, and uses of radar data received at NRL. COAMPS® and COAMPS-OS® are registered trademarks of the Naval Research Laboratory.

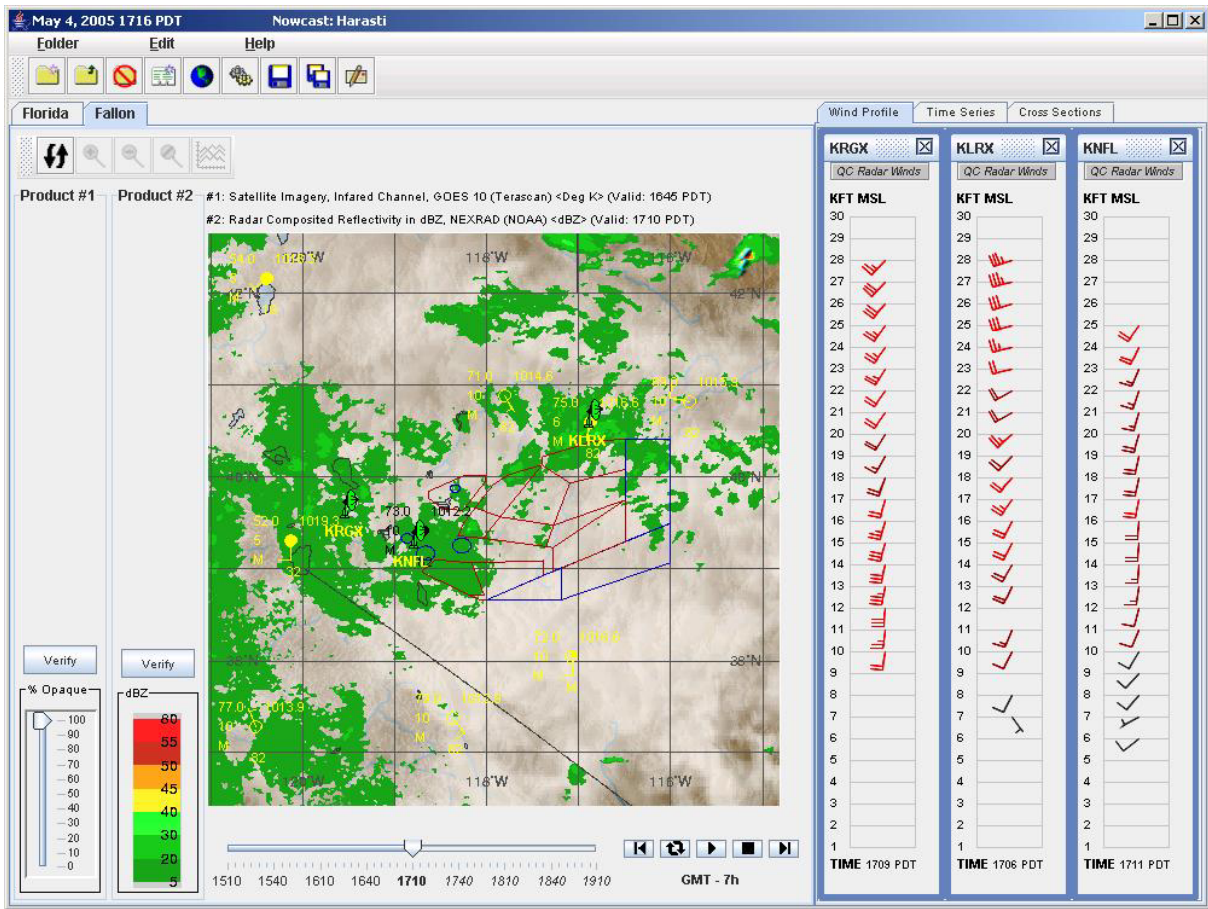


Fig. 2. NRL–NOWCAST Example: The US Naval Air Station, Fallon-Area (red and blue polygon regions) showing real-time surface observations, satellite data, and NRL quality controlled radar products (composite reflectivity and VAD radar winds from KNFL (Fallon, NV, SWR), KRGX (Reno, NV, WSR-88D) and KLRX (Elko, NV, WSR-88D).



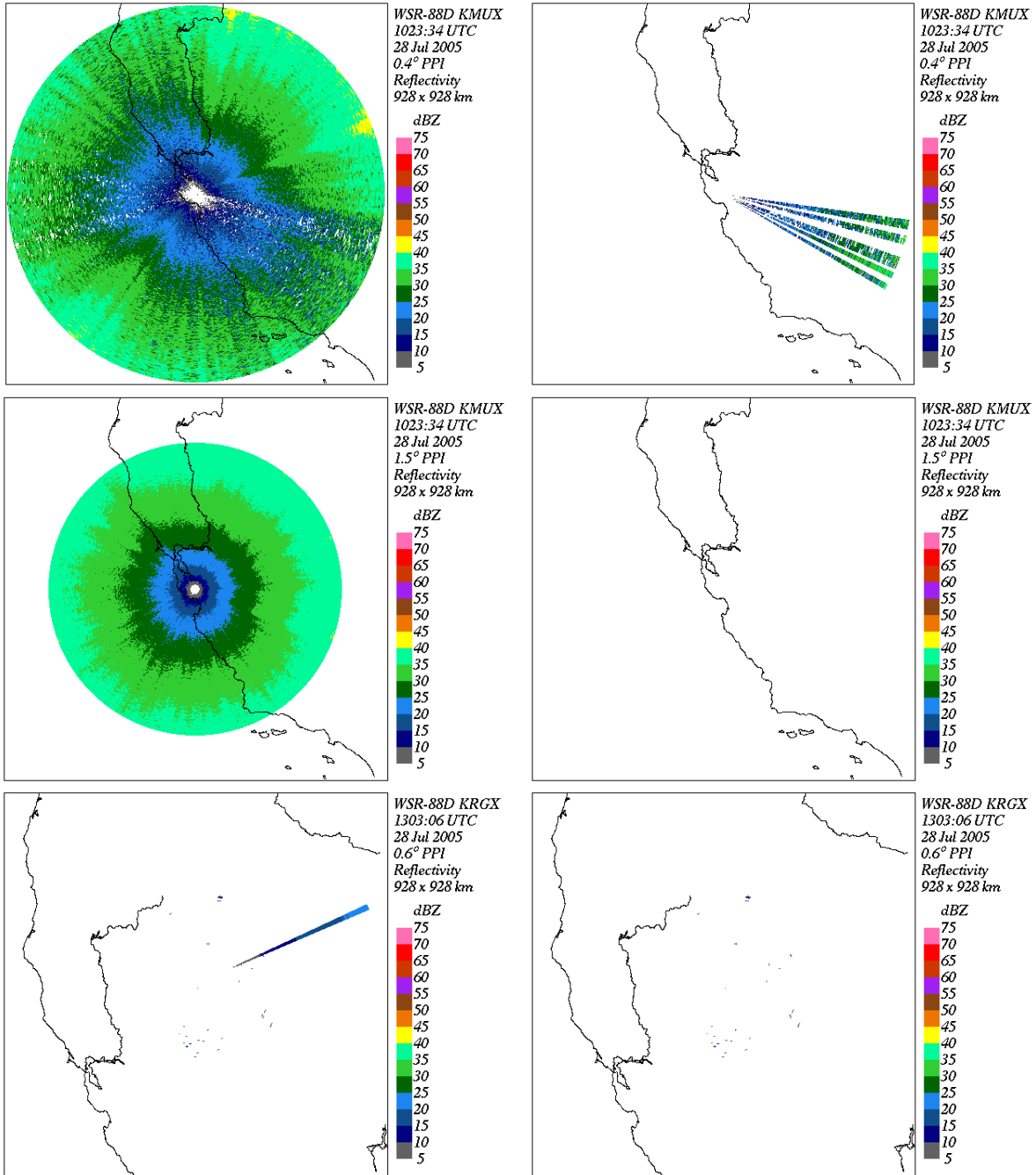


Fig. 3. CPF artifact identification and removal. Left Panel: Bull's eye reflectivity patterns from the WSR-88D at San Francisco, CA (KMUX), 1023 UTC 28 July 2005 from the 0.5° (top) and 1.5° (middle) elevation surveillance scans. A sun strobe reflectivity pattern during sun rise observed by the WSR-88D at Reno, NV (KRGX), 1303 UTC 28 July 2005 is shown at the bottom. The radar is located at the center of the image in each case, with the Pacific Ocean shoreline shown at the left, and major rivers shown elsewhere. Right panel: the results of applying the DQA CPF detector to the corresponding data shown in the left panel.

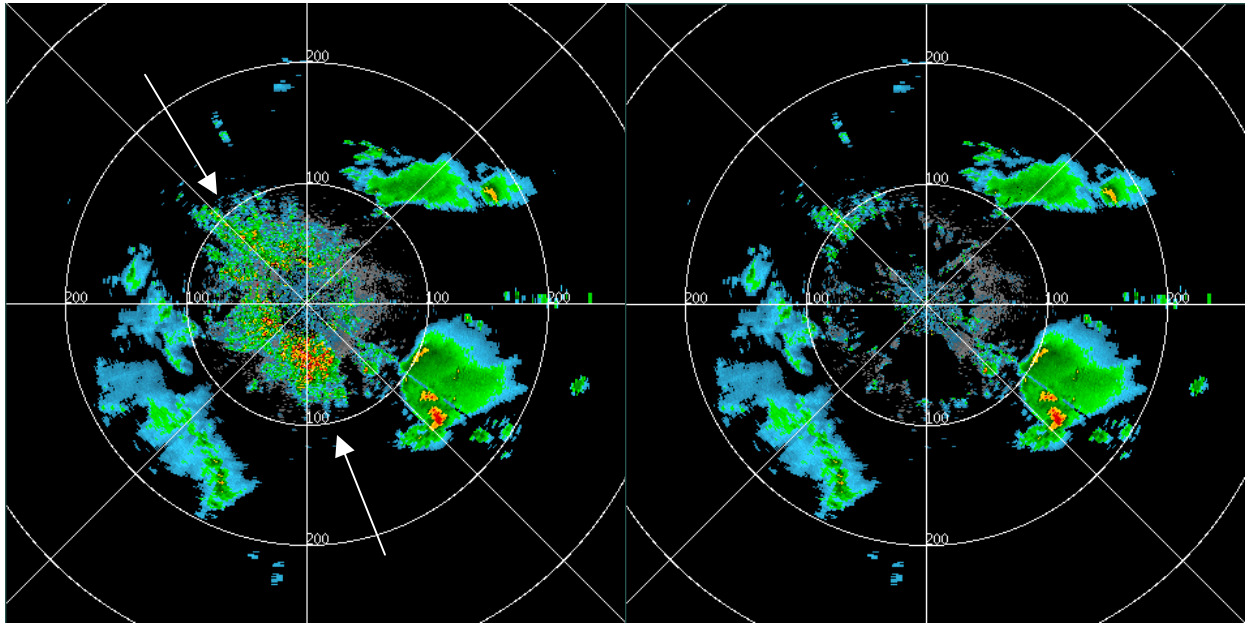


Fig. 4. AP clutter case from the WSR-88D at KAMA, TX, 0322 UTC May 25 1994. Raw reflectivity data from the 0.5° elevation surveillance scan is shown on the left. The reflectivity edited by the DQA AP detector is shown on the right. Note that most of the AP clutter shown between the two white arrows on the left is removed.

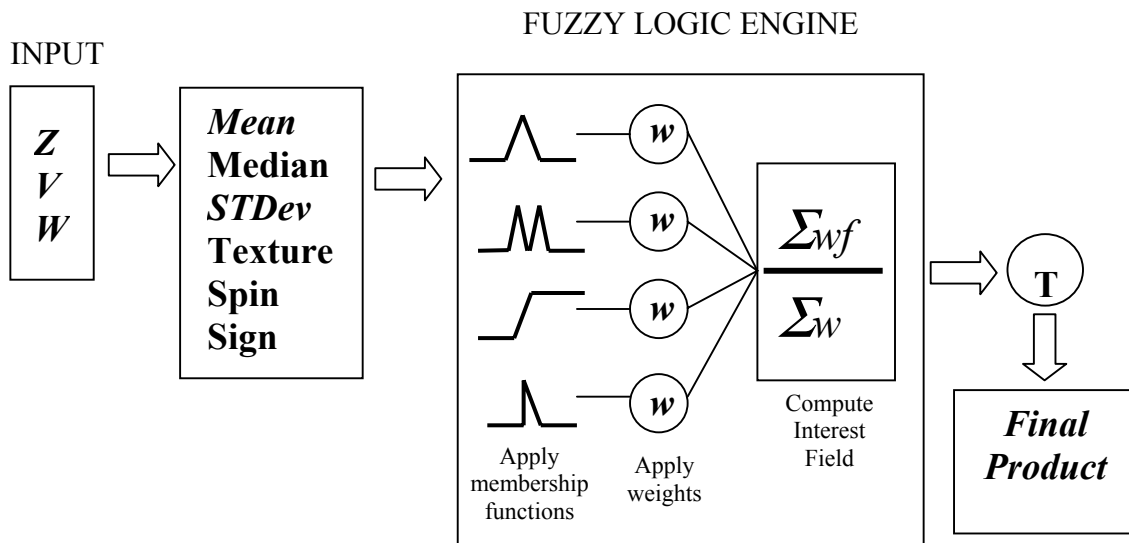


Fig. 5. General schematic of the algorithms within the NCAR REC. The steps of the process include: ingesting the base data for reflectivity ( $Z$ ), radial velocity ( $V$ ), and spectrum width ( $W$ ), generation of features that are derived from the base data fields, use of a fuzzy logic engine to determine the initial interest output, application of the appropriate threshold ( $T$ ), and the final output product for the type of radar echo being considered.

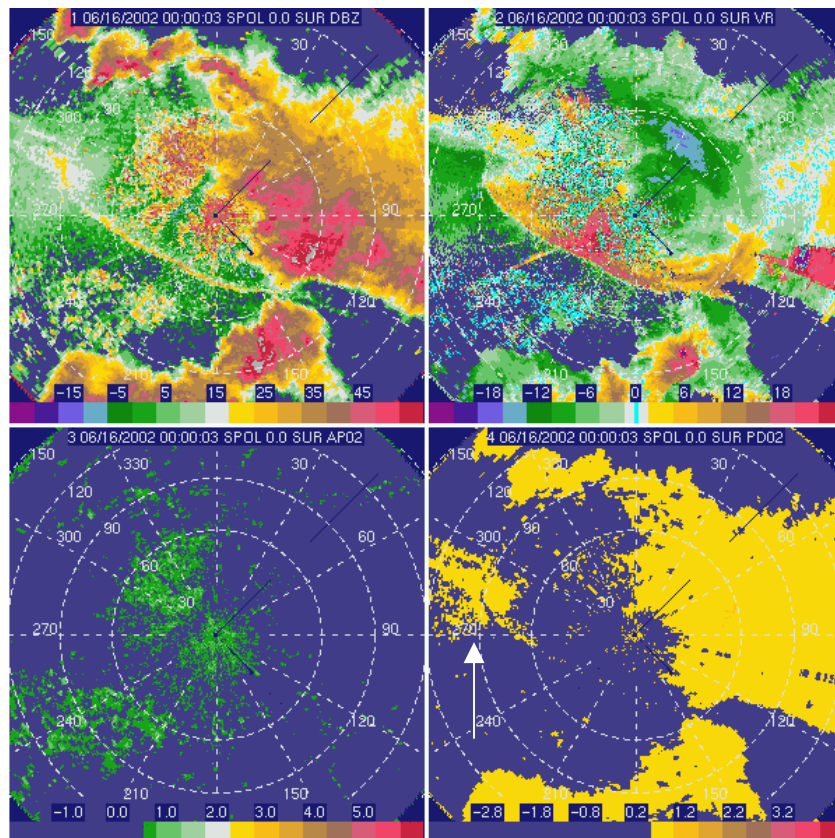


Fig. 6. REC results from the S-Pol data of the IHOP field experiment, 0000 UTC 16 June 2002. Top panel: Reflectivity in units of dBZ (left), and radial velocity in units of  $m s^{-1}$  (right) with values near zero shaded cyan. Bottom panel: Thresholded APDA shown in green (left) and thresholded PDA shown in gold (right), where the white arrow denotes a region of clear air return that is incorrectly classified as precipitation. The 0.0-degree elevation angle is shown. Range rings are at 30 km intervals.

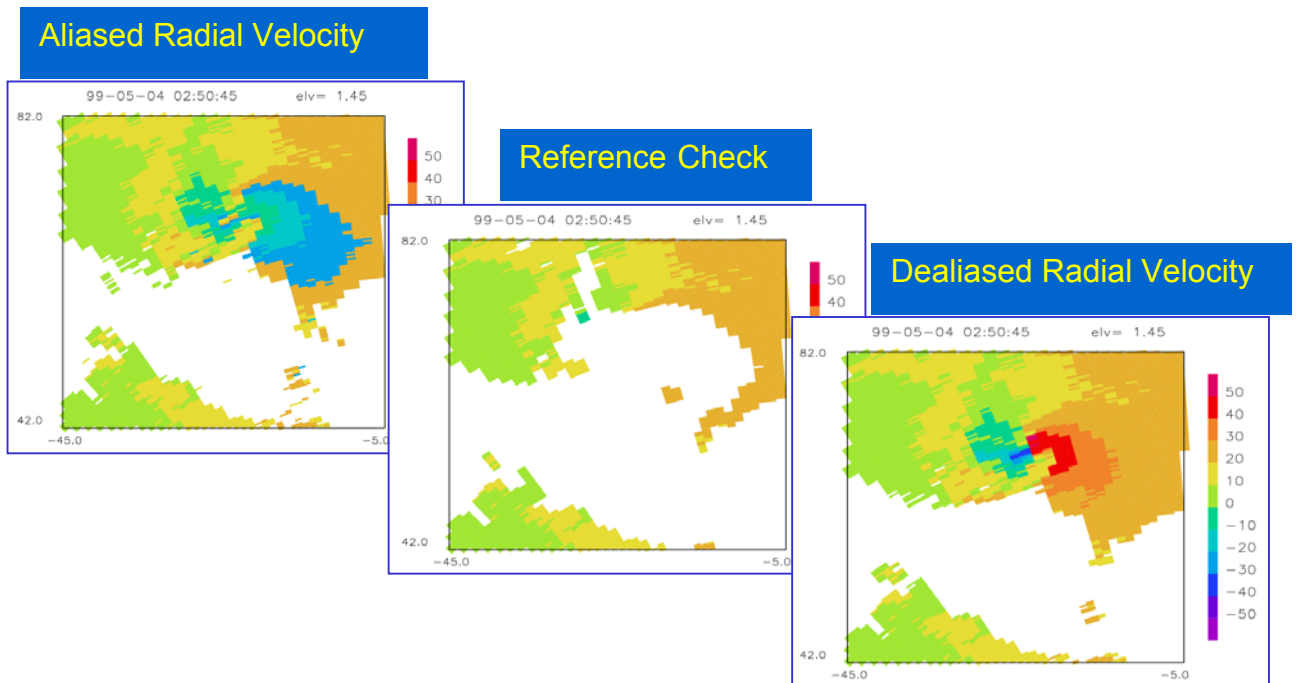


Fig. 7. Example of three-step de-aliasing algorithm of Gong et al. (2003). The left image shows the raw radial velocity of a mesocyclone observed by the KTLX WSR-88D, 1.45° elevation scan at 0250 UTC on 1999 May 4. The three steps are depicted from left to right as follows: 1) Modified VAD winds, derived from aliased data, used as reference for the first de-aliasing pass. 2) Traditional VAD winds, derived after step 1, used as new reference; remaining data jump points confined to small areas. 3) Reference check area in Step 2 used for a continuity check from all directions around flagged areas to de-alias data within these areas – the final result is the image on the right.

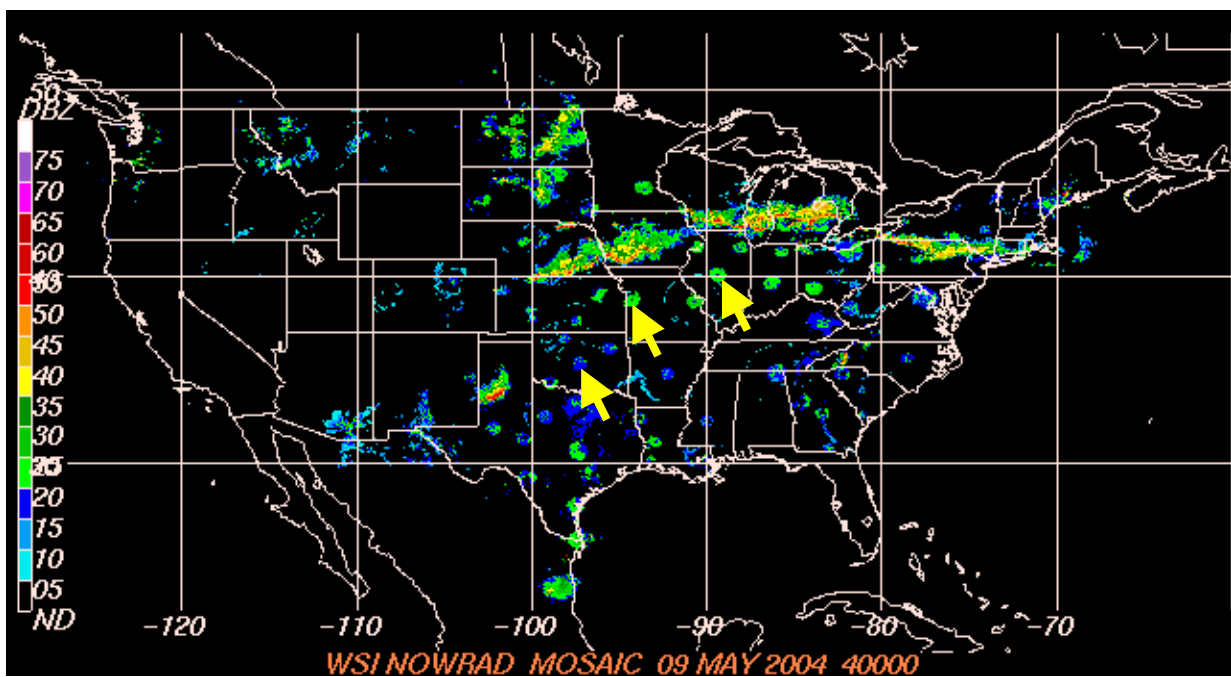
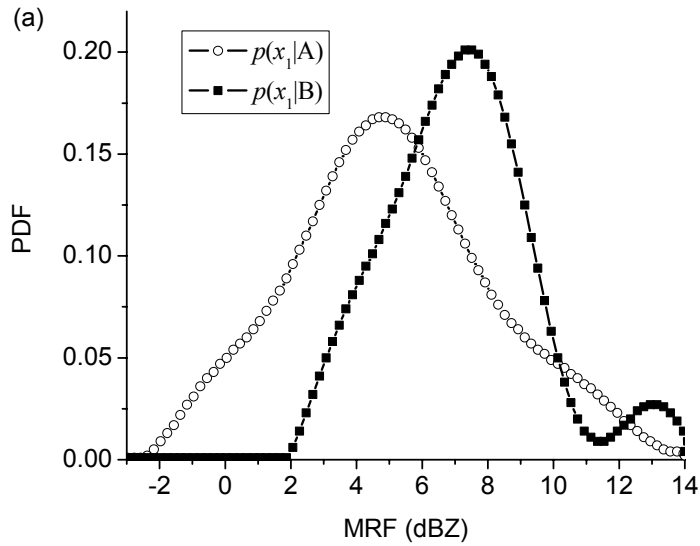


Fig. 8. Most of the circular-shaped WSR-88D reflectivity echoes shown above are migrating birds (some indicated by yellow arrows). Birds can be a very widespread problem, depending on the time of day and year (see <http://www.npwrc.usgs.gov/resource/othrdata/migratio/migratio.htm>).



(b)

Verification Parameter Type	Multi-parameter (combined MRF, VDC, and VSC) Statistic
Hit Rate	94.6%
False Alarm Rate	37.2%

Fig. 9. a) Example of the probability distribution functions for MRF. A legend is inset indicating the style of the curve for the conditional probability that the radar echo is not contaminated by birds (A), given  $x_1$ =MRF, and the conditional probability that the radar echo is contaminated by birds (B), given  $x_1$ =MRF. b) Multi-parameter verification statistics.

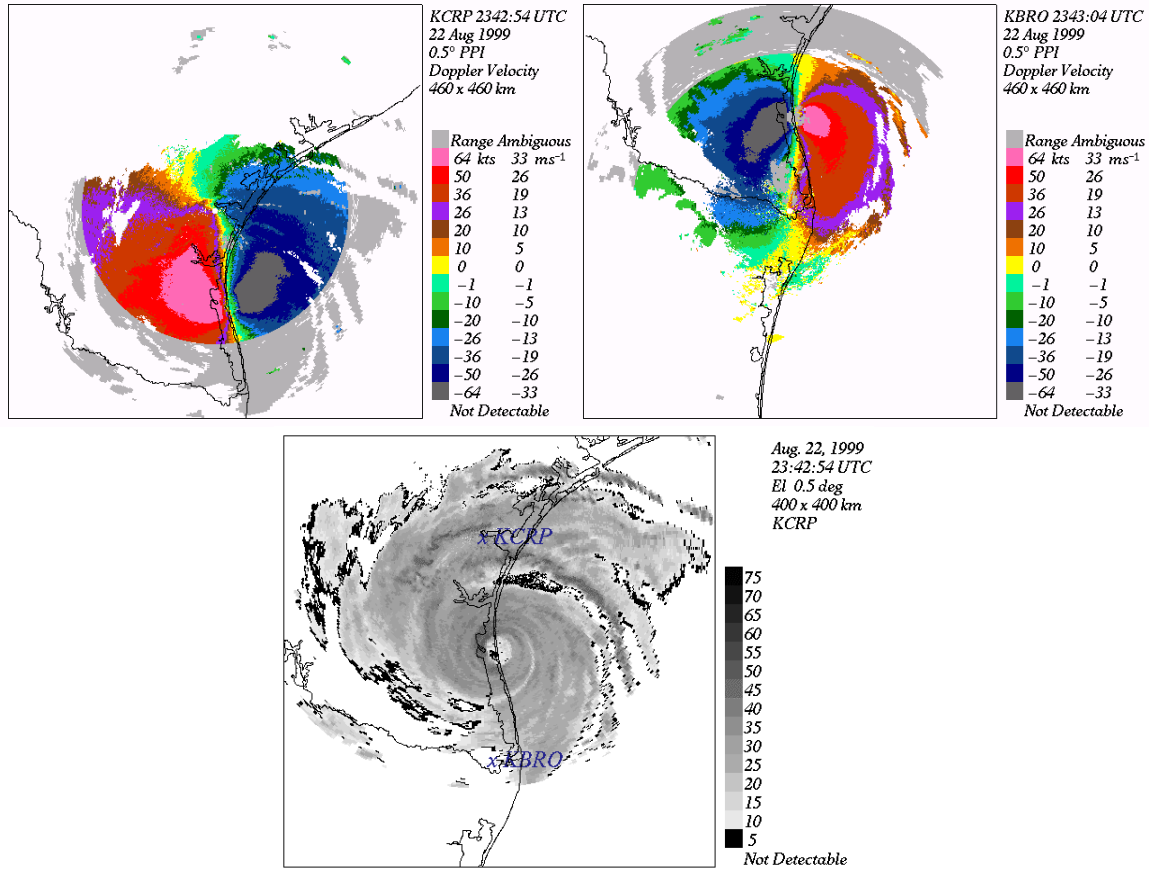


Fig. 10. Example images of the data from the 0.5° elevation scans from WSR-88D radars that observed Hurricane Bret (1999) during landfall nearly simultaneously around 2343 UTC. Top panel: radial velocity data from KCRP (left) and KBRO (right) with each radar located at the center of the image. Bottom: reflectivity data (dBZ) from KCRP, with Bret's eye near the center of the image, and the positions of KCRP and KBRO indicated by blue-colored "x" labels.



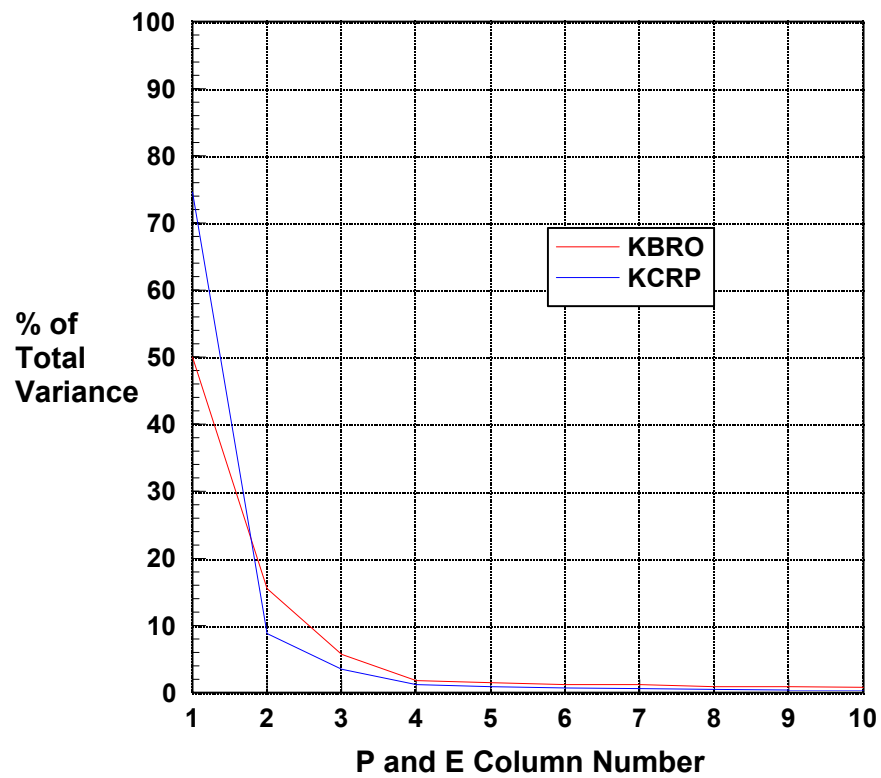


Fig. 11. Percentage of the total variance of  $\mathbf{D}$  represented by the outer product of each principal component-eigenvector pair, indexed by their column number in  $\mathbf{P}$  and  $\mathbf{E}$ . The curve legend indicates results from the PCA of the  $\mathbf{D}$  matrices whose data are depicted in the top panel of Figure 10.

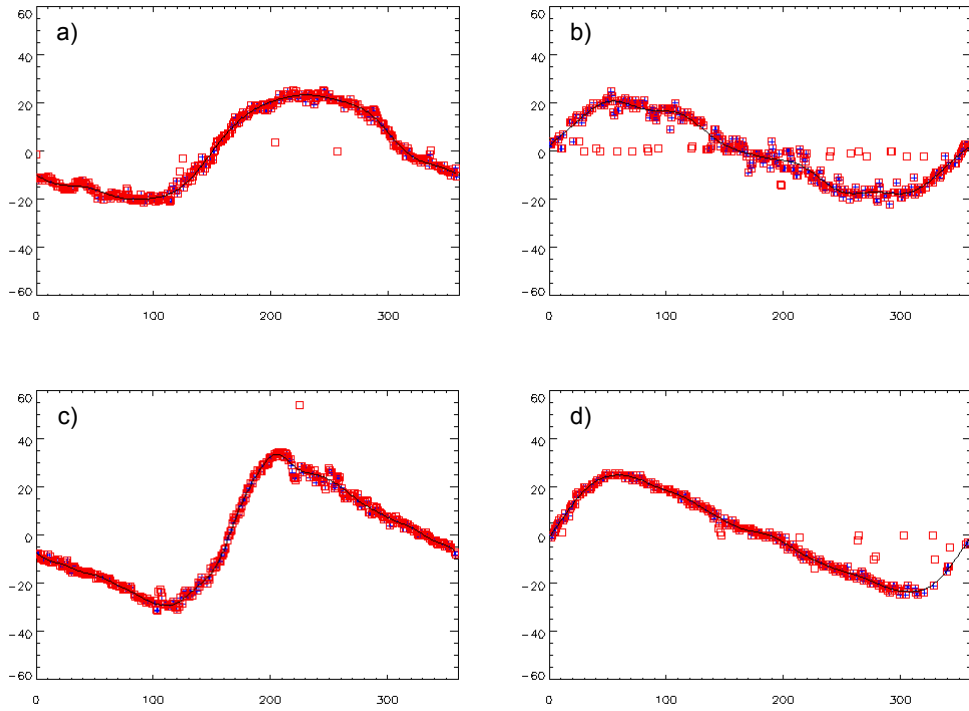


Fig.12. Radial velocity (vertical axes) versus azimuth angle (horizontal axes) plots from the KCRP (left panel) and KBRO (right panel)  $0.5^\circ$  elevation scans at fixed radar range a) 20 km, b) 21 km, c) 50 km and d) 36 km. The blue curve represents a high-order VAD fit to the radial velocity data excluding the data rejected as either clutter or noise using the PCA synthesis equation (1) and the outlier rejection criteria. Retained radial velocity data points are red-colored squares filled with blue-colored crosses; rejected data points are unfilled, red-colored squares. Note the ground clutter of near-zero radial velocity correctly identified and rejected in a)-b) and d), and the obvious noise outlier automatically detected and rejected by the PCA QC of c).

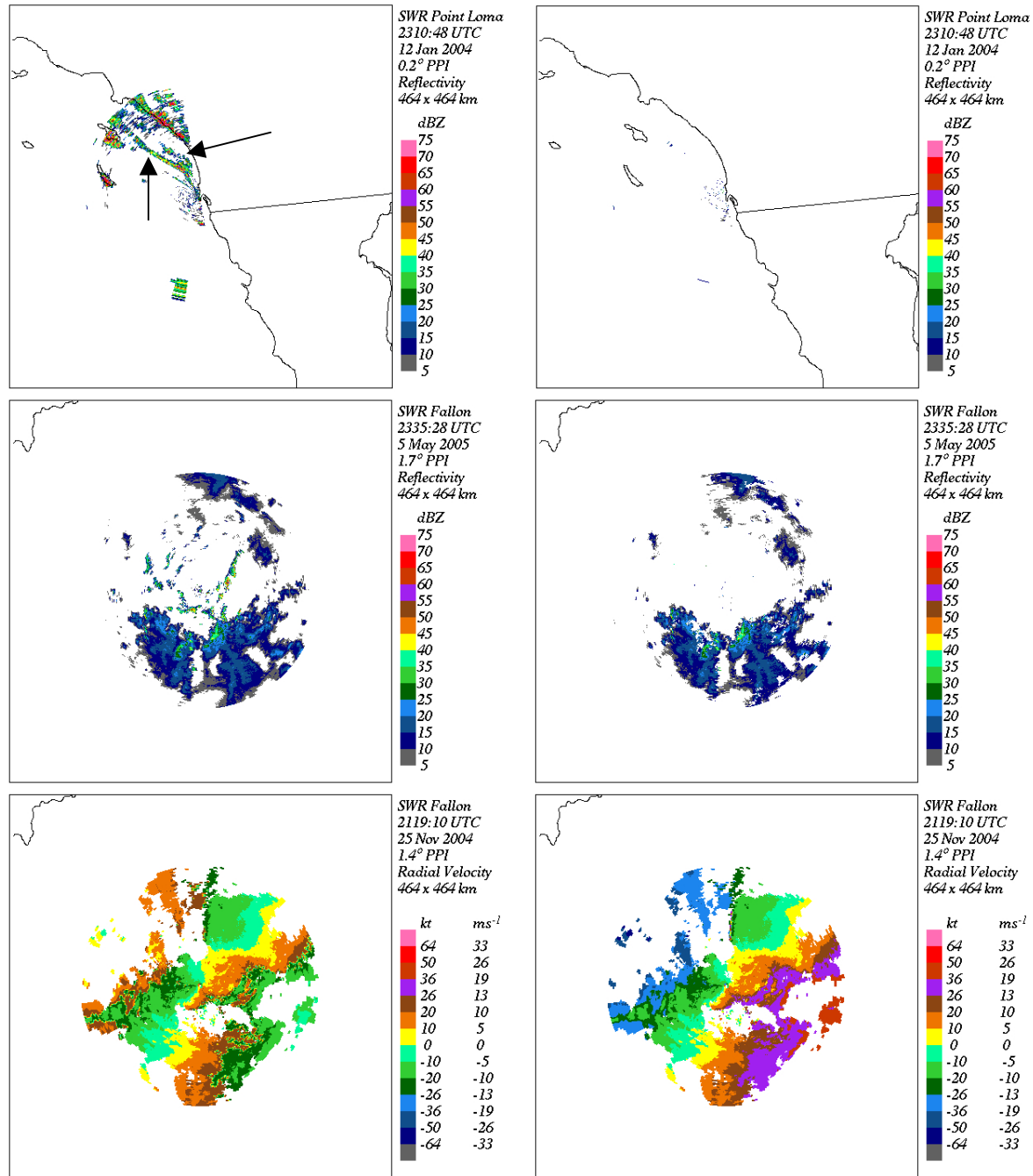


Fig. 13. Examples of applications of the current NRL QC approach to SWR data from Point Loma, CA (top panel) and Fallon, NV. The SWR is located at the center of the image in each case with major rivers and coastlines, and the US-Mexico border for the case of the top panel, shown in black. The raw data is shown in the left panel, and the corresponding QC data is shown in the right panel. The top panel shows an example of the successful removal of anomalous propagation (AP) ground and sea clutter, and two lines of second trip echoes, indicated by black arrows, from AP clutter of the distant mountains, with no weather signal present. The data removed in the middle panel are largely normal propagation ground clutter from the mountains surrounding Fallon with the majority of the weather signal from rain showers left remaining. The bottom panel shows results of the first application of the current NRL de-aliasing algorithm to radial velocity data of another rain shower event, where the Nyquist velocity was only  $13.25 \text{ m s}^{-1}$ .

Table 1. Summary of the echo target types of each of the radar data QC algorithms under consideration.

<b>Method</b>	<b>Ground Clutter</b>	<b>Precipitation</b>	<b>Insects - Clear Air</b>	<b>Sea Clutter</b>	<b>Noise</b>	<b>Birds</b>	<b>CPF Artifacts</b>
MIT/LL DQA	X						X
NCAR REC	X	X	X	X			
NSSL QC	X			X	X	X	
PCA QC	X	X			X		
NRL QC	X			X	X		